Appl. Math. Mech. -Engl. Ed., **44**(10), 1629–1650 (2023)

APPLIED MATHEMATICS AND MECHANICS (ENGLISH EDITION)

https://doi.org/10.1007/s10483-023-3038-6

Effects of time-delayed vibration absorber on bandwidth of beam for low broadband vibration suppression*

Xiuting SUN, Yipeng QU, Feng WANG, Jian XU†

School of Aerospace Engineering and Applied Mechanics, Tongji University, Shanghai 200092, China

(Received Jun. 11, 2023 / Revised Aug. 16, 2023)

Abstract The effects of time-delayed vibration absorber (TDVA) on the dynamic characteristics of a flexible beam are investigated. First, the vibration suppression effect of a single TDVA on a continuous beam is studied. The first optimization criterion is given, and the results show that the introduction of time-delayed feedback control (TDFC) is beneficial to improving the vibration suppression at the anti-resonance band. When a single TDVA is used, the anti-resonance is located at a specific frequency by the optimum design of TDFC parameters. Then, in order to obtain low-frequency and broad bands for vibration suppression, multiple TDVAs are uniformly distributed on a continuous beam, and the relationship between the dynamic responses and the TDFC parameters is investigated. The obtained relationship shows that the TDVA has a significant regulatory effect on the vibration behavior of the continuous beam. The effects of the number of TDVAs and the nonlinearity on the bandgap variation are discussed. As the multiple TDVAs are applied, according to the different requirements on the location and bandwidth of the effective vibration suppression band, the optimization criteria for the TDFC parameters are given, which provides guidance for the applications of TDVAs in practical projects such as bridge and aerospace.

Key words time-delayed vibration absorber (TDVA), time-delayed feedback control (TDFC), parameter design criterion, broadband vibration suppression

Chinese Library Classification O342
2010 Mathematics Subject Classification 74K10

1 Introduction

Vibration suppression techniques[1] have attracted extensive research interests, since the existence of vibration with low-frequency and large amplitude may lead to failures of engineering structures[2], errors in manufacturing processes[3], discomforts of transportation[4], etc. Dynamic vibration absorber is significant for the effective suppression of undesired vibrations[5–6].

∗ Citation: SUN, X. T., QU, Y. P., WANG, F., and XU, J. Effects of time-delayed vibration absorber on bandwidth of beam for low broadband vibration suppression. *Applied Mathematics and Mechanics* (*English Edition*), **44**(10), 1629–1650 (2023) https://doi.org/10.1007/s10483-023-3038-6

† Corresponding author, E-mail: xujian@tongji.edu.cn

Project supported by the National Natural Science Foundation of China (Nos. 12122208, 11972254, and 11932015)

A traditional vibration absorber usually consists of a mass, a spring, and a damper, as a tuned-mass-damper (TMD)[7–8]. Since TMD is effective in the application of vibration suppression at a fixed excitation frequency, which strictly equals the natural frequency of the primary system to induce the anti-frequency point, its effective frequency band is so narrow that it is not practicable to suppress the vibrations for cases with varying excitation frequencies. Thus, variable semi-/active control methods are carried out to improve the performances of vibration absorbers[9–13].

In active control methods, time delay is unavoidable in active control loop due to the data acquisition, signal transmission, mathematical calculation, and force actuation cost time. In the early studies, time delay was considered as an unexpected parameter because it might lead to errors in the control results, destabilization of systems, chaotic phenomena, etc. In order to eliminate the negative factor, many compensation methods of time delay were proposed[14–15]. With the deepening of research, time delay has been proved to be effective in the control of various dynamic systems. Researchers have found that time delay is effective in the stabilization of unstable periodic orbits embedded in chaotic attractors[16], the chaos synchronization of dynamic systems[17], the balancing of wheeled inverted pendulums[18–19], the vibration reduction of flexible beams[20–21], chatter and flapping[22–23], etc. Time-delayed feedback control (TDFC) is treated as a novel control technique due to its capability for adjusting the frequency and amplitude according to the requirements in variable vibration control problems. Sun and Xu[24] and Sun et al.[25–26] studied the multi-directional quasi-zero-stiffness with multiple time delays in low-frequency vibration suppression for nonlinear systems. El-Sayed and Bauomy[27] and Saeed and El-Ganaini[28] obtained the optimum control parameters for problems with impact and harmonic excitations to improve the performances of TDFC, and showed that TDFC was suitable for vibration isolation due to its ability to tune the stiffness and damping properties of isolators, especially for low-frequency ranges. Yang and Cao[29–30] studied the displacement and velocity feedback with time delay to control the vibration of a smooth and discontinuous (SD) oscillator with nonlinear stiffness, and established the relationship between the parameters and the vibration characteristics of the SD oscillator with nonlinear stiffness. It is pointed out that, from a physical point of view, the TDFC adjusts the equivalent stiffness and damping characteristics, and optimizes the effect of vibration control.

Since TDFC has the capacity of adjusting equivalent stiffness and damping, it has been introduced to vibration absorber for better vibration absorption. Olgac and Holmhansen[31] proposed the first design of time-delayed vibration absorber (TDVA), which was defined as delayed-resonator (DR). The time-delayed displacement was utilized as the feedback control signal to suppress the vibration of a linear dynamic system. The results showed that the introduction of TDFC was capable of tuning the vibration responses of the primary system. With the chosen control parameters, the vibration of the primary system could be totally eliminated. In engineering applications, the primary system may be subject to external excitations with multiple sinusoidal harmonics. In view of the design problem of TDVA in the case of multi-frequency external excitations, Olgac et al.[32] proposed two design methods for TDVA, and mainly discussed the design and function of the dual-frequency fixed DR. The results showed that the natural frequencies of the vibration absorber and the external excitation frequencies could be exactly equal by a reasonable selection of the control gain and time delay, and the response of the main system at the two frequencies could be completely absorbed by the TDVA simultaneously. Jalili and Olgac[33] adopted multiple identical TDVAs for the vibration suppression of multi-degree-of-freedom systems, and showed that the reduction of vibrations for several masses of the primary system could be significantly improved. Hosek et al.[34–35] proposed the centrifugal time-delay resonator to suppress torsional vibration, and used the proportional angular-displacement feedback control with variable time-delay to achieve the full absorption of the structure torsional vibration. Sun and Xu[36] and Xu and Sun[37] designed a TDVA for the vibration of a linear system, and used the acceleration signal to achieve anti-resonance phenomena. The results showed that the TDVA was suitable for the vibration suppression of linear systems. Wang and Xu[38] and Wang et al.[39–40] proposed the parameter design criteria for TDVAs based on an anti-resonance frequency analysis for linear and nonlinear systems. The theoretical and experimental results showed that the proposed TDVAs were effective in the vibration suppression of both linear and nonlinear primary systems. Zhang et al.[41–42] studied TDVAs with friction, and discovered that the stability mode was related to the excitation frequency due to the existence of non-smooth friction model. Besides, the corresponding experiment of TDVAs determined the value of time delay in the control loop[42]. Meng et al.[43–44] utilized the nonlinear TDVA to achieve equal-peak phenomena. Ji and Zhang[45–46] analyzed the vibration suppression effects of the TDVA on the primary and super-harmonic resonances of the nonlinear primary system, and clarified the effectiveness of the TDVA on the above vibration suppression.

For broadband vibration suppression of flexible beams, multiple vibration absorbers have been adopted as inner local resonators (LRs) to form quasi-periodic structure. Owing to their unusual properties such as negative effective mass density and stiffness, acoustic meta materials have been employed for the vibration isolation and absorption in a broad low-frequency range[47–52]. Various design principles have been proposed for LRs based on the width of bandgaps with/without active control[53–57]. However, there still exist contradictions on the design and optimization of dynamic behaviors. Although the location of the bandgap can be decreased to the low-frequency range, the width of it is reduced. The width of the vibration bandgap can be increased, and the resonance peak can be reduced by increasing the coupling damping, but the amplitude in the effective band is increased at the same time. To break the limitation, control mechanisms are needed to achieve adjustable bandgaps for applications in various external environments. Practically, TDVA, made up of a mass-spring-damper and a delayed-controller, has been proven to be able to provide adjustable stiffness and damping simultaneously[58–59]. Therefore, TDVA is expected to provide a potential path to realize the vibration suppression within a wide low-frequency range for flexible beams.

In this study, the effects of multiple TDVAs on the dynamic characteristics of a flexible beam are investigated. In Section 2, the flexible beam model with one attached TDVA is established. The frequency response function of the beam is obtained by the Galerkin truncation method, and the vibration suppression effect of a single TDVA on the beam is studied. In Section 3, the delay-coupled system of the flexible beam and multiple TDVAs, which are uniformly distributed, is proposed. The beam is considered as a quasi-periodic structure with TDVAs as the inner LRs, and the wide band vibration suppression effects are investigated. The relationship between the dynamic responses of the beam and the TDFC parameters is investigated. The relationship between the effective vibration control frequency band and the control parameters is given. In Section 4, conclusions are drawn, and discussion is made.

2 Vibration suppression effects of single TDVA

2.1 Mathematical modeling

Figure 1(a) shows a flexible beam with multiple TDVAs, and Fig. 1(b) shows a beam with one TDVA. The oscillations of the TDVA and the beam are both in the vertical direction w. The coupling force and the control force between the flexible beam and the TDVA are written as f_{d} and f_{control}, respectively. The governing equations of the flexible beam with one TDVA (see Fig. 1(b)) are written as

$$\begin{cases} EI\dfrac{\partial^4 w}{\partial x^4} + \rho A\dfrac{\partial^2 w}{\partial t^2} = f_{\mathrm{E}}(t)\delta(x - x_{\mathrm{E}}) + (f_{\mathrm{d}}(z_r, w_r, \dot{z}_r, \dot{w}_r, t) \\ \qquad\qquad\qquad\qquad + f_{\mathrm{control}}(z_r, z_{r\tau}, w_\tau, x_r, t))\delta(x - x_r), \\ m_r\ddot{z}_r(t) + f_{\mathrm{d}}(z_r, w_r, \dot{z}_r, \dot{w}_r, t) + f_{\mathrm{control}}(z_r, z_{r\tau}, w_\tau, x_r, t) = 0, \end{cases} \tag{1}$$

where E is Young's modulus, I is the moment of inertia, ρ is the density, A is the area of the cross section, $w(x,t)$ is the deflection of the beam at position x and time t, m_r is the mass of the TDVA, z_r is the vibration of the TDVA, $z_{r\tau}$ is the TDFC signal as $z_r(t-\tau)$ from the TDVA, and w_τ is the TDFC signal as $w(x,t-\tau)$ from the beam. In Eq. (1), $\delta(\cdot)$ is the Dirac delta function, $\delta(x-x_{\mathrm{E}})$ represents that the excitation is applied at x_{E}, and $\delta(x-x_r)$ represents that the TDVA is applied at x_r on the beam.

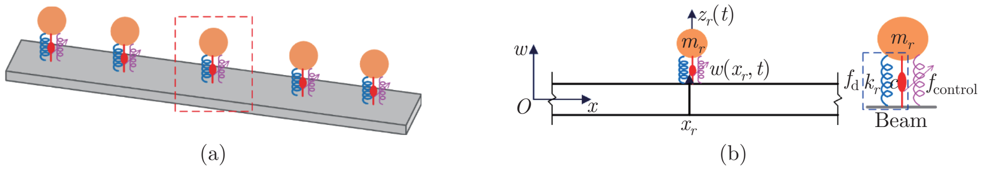

Fig. 1 (a) Flexible beam with multiple TDVAs. (b) Flexible beam with one TDVA (color online)

Based on the Galerkin truncation method, the transverse displacement of the beam can be assumed as

$$w(x,t)=\sum_{p=1}^{P}\phi_p(x)q_p(t), \tag{2}$$

where P is the total number of the Galerkin truncations, $\phi_p(x)$ is the pth modal function, and $q_p(t)$ is the pth generalized displacement. The internal force between the TDVA and the beam is

$$\begin{aligned}f(z_r,z_{r\tau},w_\tau,x_r,t)&=f_{\mathrm{d}}+f_{\mathrm{control}}\\&=k_r(z_r(t)-w(x_r,t))+c_r(\dot{z}_r(t)-\dot{w}(x_r,t))\\&\quad+gk_r(z_r(t-\tau)-w(x_r,t-\tau)).\end{aligned} \tag{3}$$

Substituting Eq. (2) into the first equation of Eq. (1) yields

$$\begin{aligned}&EI\sum_{p=1}^{P}\int_0^L\phi_p^{(4)}(x)\phi_n(x)\mathrm{d}xq_p(t)+\rho A\sum_{p=1}^{P}\int_0^L\phi_p(x)\phi_n(x)\mathrm{d}x\ddot{q}_p(t)\\&=\int_0^L\phi_n(x)\delta(x-x_{\mathrm{E}})\mathrm{d}xf_{\mathrm{E}}(t)+\int_0^L\phi_n(x)\delta(x-x_r)f(x_r,t)\mathrm{d}x.\end{aligned} \tag{4}$$

According to Fig. 1, The modal functions are selected as those for the Euler beams with free-free end boundaries. Due to the orthogonality of the modal functions and considering the modal damping of the beam and the TDVA, Eq. (4) can be formulated as

$$\begin{aligned}&m_p\ddot{q}_p+c_p\dot{q}_p+k_pq_p\\&=\phi_p(x_{\mathrm{E}})f_{\mathrm{E}}(t)+\phi_p(x_r)c_p\dot{z}_r(t)+k_r\phi_p(x_r)(z_r(t)-\phi_p(x_r)q_p)\\&\quad+gk_r\phi_p(x_r)(z_r(t-\tau)-\phi_p(x_r)q_{p\tau}),\end{aligned} \tag{5}$$

where

$$m_p=\rho A\int_0^L\phi_p^2(x)\mathrm{d}x,\quad k_p=EI\int_0^L\phi_p^{(4)}\phi_p(x)\mathrm{d}x,\quad c_p=2\zeta_p\sqrt{m_pk_p},$$

in which ζ_p is the equivalent damping ratio of the pth beam mode.

The dynamic responses of the pth generalized displacement of the beam $q_p(t)$ and the TDVA are assumed as the periodic functions written as follows:

$$\begin{cases} q_p(t) = a_p \sin(\omega t) + b_p \cos(\omega t), \\ z_r(t) = c_r \sin(\omega t) + d_r \cos(\omega t), \end{cases} \tag{6}$$

and the excitation $f_{\mathrm{E}}(t)$ is assumed as

$$f_{\mathrm{E}}(t) = f_{\mathrm{E}} \cos(\omega t).$$

Substituting Eq. (6) and the excitation into Eq. (1), one can derive $(P+2)$ equations. Then, collecting the coefficients of $\sin(\omega t)$ and $\cos(\omega t)$ and setting them as zero, one can derive $2(P+2)$ equations related to a_p, b_p, c_r, d_r, and f_{E}. Rearranging the $2(P+2)$ equations, one gets

$$\boldsymbol{C}_{2(P+2)\times 2(P+2)} \boldsymbol{A}_{2(P+2)\times 1} = \boldsymbol{E}_{2(P+2)\times 1}, \tag{7}$$

where $\boldsymbol{A}_{2(P+2)\times 1}$ $(= (a_1, b_1, \cdots, a_p, b_p, c_r, d_r)^{\mathrm{T}})$ is the vector of the generalized displacement amplitudes of cosines and sines, $\boldsymbol{C}_{2(P+2)\times 2(P+2)}$ is the matrix of the coefficients, $\boldsymbol{E}_{2(P+2)\times 1}$ is the matrix related to the excitation force. $\boldsymbol{A}_{2(P+2)\times 1}$ can be calculated according to Eq. (7). The results are substituted into Eqs. (2) and (6), and then the dynamics of the beam and LRs can be derived. The frequency response function (F_{RF}) of the beam is defined as the spectrum of the displacement at the beam end divided by that at the tip of the beam as follows:

$$F_{\mathrm{RF}} = 20 \lg(|w(L,t)|/|w(0,t)|), \tag{8}$$

where $|\cdot|$ denotes the amplitude of $(\cdot)$. In this study, the position of excitation force is assumed as the left end of the beam so that $x_{\mathrm{E}} = 0$, and the position of TDVA is at the right end of the beam and $x_r = L$.

2.2 Vibration suppression effects of TDVA

The physical parameters of the proposed beam are listed in Table 1. The material of the beam is chosen as aluminum. The cross section of the beam is a rectangle with the width of 0.03 m and the height of 0.012 m. The length of the beam is fixed as 1 m. In the following analysis, the default number of the unit cells of the beam is chosen as 8, and the mass of the TDVA m_r is assumed as 20% of the mass of one unit cell. Similarly, when the unit cell number of the beam is chosen as 4, the mass m_r of the TDVA is 10% of the mass of one cell. The stiffness of the coupling spring between the TDVA mass and the beam is chosen as 8 000 N/m.

Table 1 Physical parameters of the flexible beam and TDVA

Parameter	Description	Value
E	Young's modulus of beam	70 GPa
ρ	Density of beam	2 700 kg/m^3
I	Moment of inertia of beam	4.32×10^{-9} m^4
A	Area of cross section of beam	3.6×10^{-4} m^2
L	Length of beam	1 m
m_r	Mass of TDVA	0.025 kg
k_r	Stiffness of TDVA	8 000 N/m
ζ_p	Modal damping ratio of beam	0.02
ζ_r	Damping ratio of TDVA	0.01
f_{E}	Amplitude of excitation force	1 N

2.2.1 Effects of control gain (cases without time delay)

To clarify the effects of the control gain on the vibration amplitude and effective vibration suppression frequency bands, the time delay is set as zero. In Fig. 2, the results of F_{RF} at the end of the beam under different control gains g are shown.

From Fig. 2, it can be seen that there always exists an anti-resonance frequency point between the first and second peaks, at which the response at the end of the beam is the lowest. In the cases shown in Fig. 2, when the control gain g increases from -0.9 to 0.9, the anti-resonance frequency of the beam increases from 29.16 Hz to 123.56 Hz.

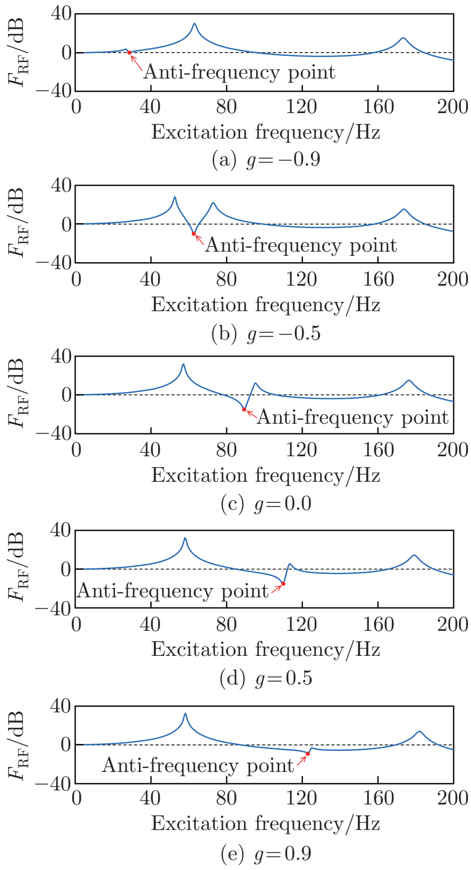

Fig. 2 Results of F_{RF} at the end of the beam for different control gains g (color online)

For no active control (see Fig. 2(c)), since the natural frequency of the TDVA without active part is about 90 Hz, which approximately equals $\sqrt{k_r/m_r}$ $(=\sqrt{8\,000/0.025}=565.7\,\mathrm{rad/s}=90.07\,\mathrm{Hz})$, the anti-resonance frequency point is around 90.05 Hz. When the control gain is negative (see Figs. 2(a) and 2(b)), the anti-resonance point is reduced to less than 90 Hz. When the control gain is positive (see Figs. 2(d) and 2(e)), the anti-frequency point is tuned over 100 Hz. Unfortunately, when the time-delay equals zero, the response amplitude at the anti-frequency point under either a negative or a positive control gain is larger than that under $g=0$. Thus, the results in this section demonstrate that the feedback control without time delay deteriorates the vibration suppression for the response amplitude at the anti-frequency point.

Therefore, the time delay should be introduced into the feedback control and the influence of time delay on the dynamic responses should be studied by defining the corresponding optimization criteria of the time-delayed control parameters.

2.2.2 Effects of time delay

In order to explore the effects of time delay on the dynamic response of the beam, in Fig. 3, the results of F_{RF} at the end of the beam for different time delays under $g = -0.2$ and 0.2 are presented. From Fig. 3, it can be seen that when the control gain g is fixed, the dynamic behavior of the beam can be adjusted by adjusting the time delay. For the case with negative control gain (see Fig. 3(a)), when the time delay increases from 0 ms to 6 ms, the anti-frequency point increases from 80 Hz to 100 Hz, and the amplitude at the anti-frequency point is non-monotonic. For the other case with positive control gain (see Fig. 3(b)), when the time delay increases from 0 ms to 5.5 ms, the anti-frequency point is reduced to lower frequency band. The amplitude at the anti-frequency point for the case as $\tau = 5.5$ ms is much less than that of the case as $\tau = 0$ ms. Therefore, by means of adjusting the time delay, the anti-frequency point can be varied for both lower and higher frequencies, which induces adjustable optimum vibration suppression property.

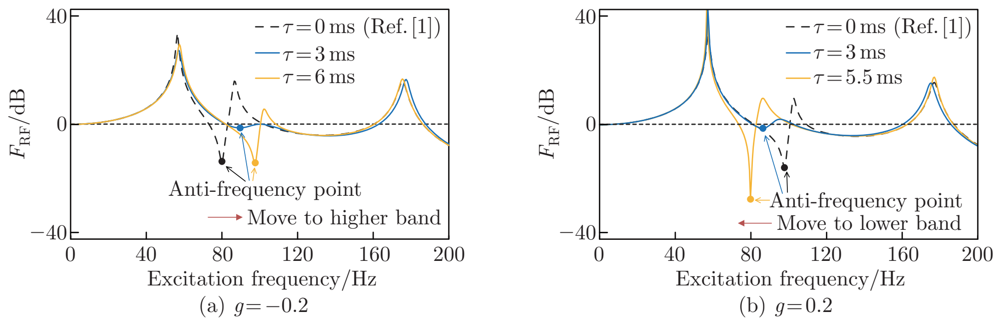

Fig. 3 Results of F_{RF} at the end of the beam with different time delays under different control gains g (color online)

Therefore, it can be concluded that different time delays correspond to different anti-resonance frequencies. Besides, the response amplitude of the beam at the anti-resonance greatly depends on the value of the time delay.

From the results shown in Fig. 3, it can be discovered that the variations of the anti-frequency point and response amplitude are non-monotonic. We propose the optimization criterion R to obtain the TDFC parameters for two conditions, the anti-frequency point Ω_{a} should be fixed at the specified point Ω_{f}, and the response amplitude a should be reduced to the lowest level at the anti-frequency point, i.e.,

$$R = \{(g, \tau) | \Omega_{\mathrm{a}} = \Omega_{\mathrm{f}} \& \min(a_{\Omega_{\mathrm{a}}})\}, \tag{9}$$

where $a_{\Omega_{\mathrm{a}}}$ is the response amplitude at the anti-frequency point.

According to the optimal criterion for one TDVA as given in Eq. (9), the optimal control gain g and time delay τ under different external excitation frequencies are calculated (see Fig. 4).

In Fig. 4(a), in the frequency band of $[75, 115]$ Hz, the variation of the optimal control gain g is approximately a straight line, and there is a jump at 107 Hz. When the external frequency is less than 90 Hz, the optimal control gain g is positive. When the external frequency is beyond 90 Hz, the optimal control gain g is negative. When the excitation frequency equals 90 Hz, the optimal value of g is zero. For the optimal values of time delay (see Fig. 4(b)), the variation of the optimal time delay τ is non-monotone and nonlinear. At 90 Hz and 109 Hz, there exists jumping for the optimal τ. The optimal τ varies quasi-periodically, since the time-delayed control affects the equivalent stiffness and damping properties with respect to the time delay.

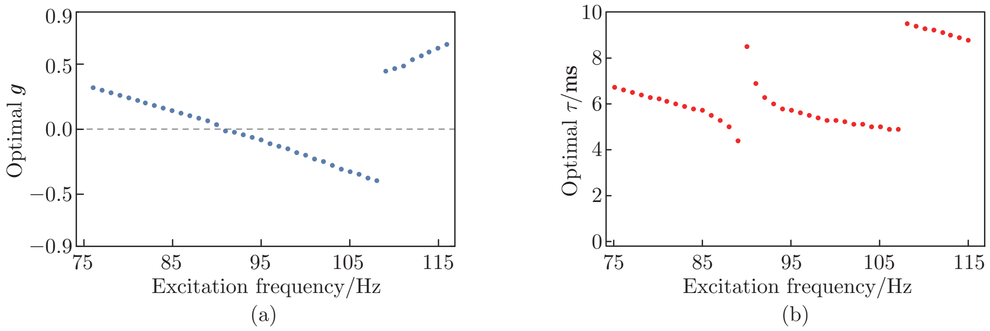

Fig. 4 Optimal values of the control gain g (a) and the time delay τ (b) under different external excitation frequencies (color online)

The beam F_{RF} results without control, with control restrained by zero time delay, and with the optimal TDFC are shown in Fig. 5. From the black dashed lines shown in Fig. 5, we can see that the anti-frequency point is located at 90 Hz for the case without control ($g = 0.0$ and $\tau = 0.0$ ms). In addition, without time delay ($\tau = 0.0$ ms), the anti-frequencies under different control gains can be adjusted to the required values according to the classical control method[1], but the response amplitude at the anti-frequency point cannot be further reduced. As $g = 0.2$, 0.0, -0.2, and 0.5, the anti-frequencies are 80 Hz, 90 Hz, 100 Hz, and 110 Hz (see the blue solid lines in Fig. 5). When time delay is considered ($\tau > 0.0$ ms) and the optimal TDFC parameters are applied, not only the anti-frequency can be adjusted, but also the amplitude at the anti-frequency can be further reduced (see the yellow solid lines in Fig. 5). Thus, the TDVA

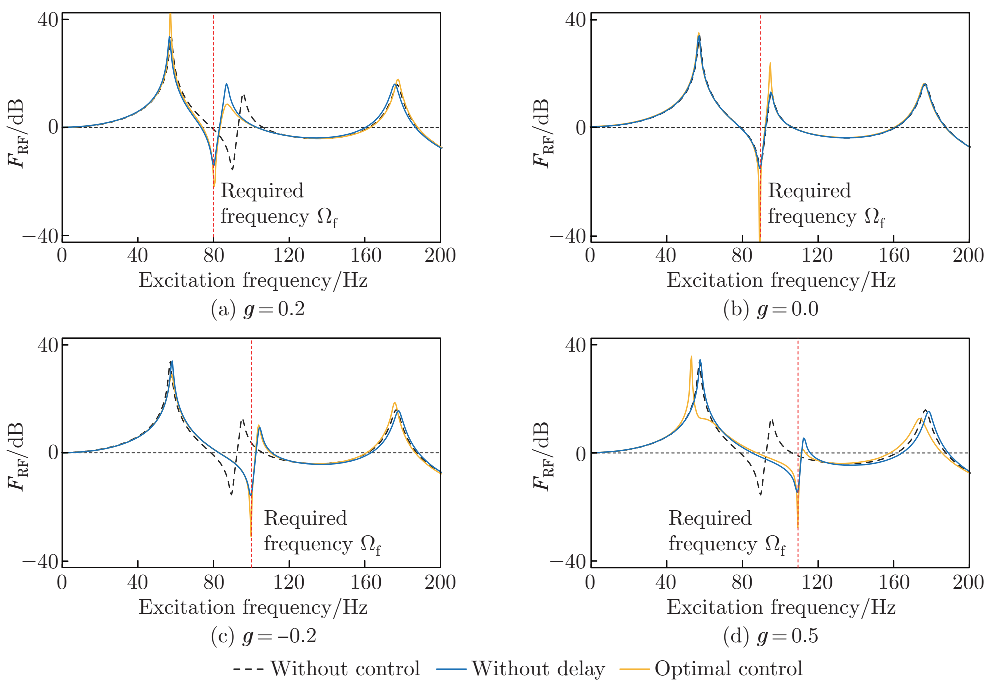

Fig. 5 Results of the beam F_{RF} without control, with optimal gain and zero-time delay, and with the optimal TDFC under different control gains g (color online)

designed by the optimal criterion of Eq. (9) can significantly reduce the response of the beam at the required external excitation frequency, since time delay can adjust not only the equivalent coupling stiffness but also the equivalent damping property. From Fig. 5, we can also see that the TDFC can change the anti-resonance frequency of the beam in a wide frequency band, and improve the vibration suppression of the beam at the anti-resonance frequency.

In this section, the influence of a single TDVA on the dynamic response of the beam is studied. The influence rules of TDFC on the dynamic response of the beam are given. It is found that the anti-resonance frequency of the beam can be changed by adjusting the TDFC parameters. Through numerical calculations, the relationship between the optimal control gain and time delay and the given external excitation frequency is given. Based on the comparison of the responses of the beam among the cases without control, with the optimal control gain without time delay, and with the optimal TDFC parameters, it is found that the TDFC can greatly improve the suppression effect of the vibration absorber on the dynamic response of the beam. The research in this section provides a reference for the application of single TDVA in the vibration suppression of beams.

3 Vibration suppression effects of multiple TDVAs

From the analysis above, it has been verified that one TDVA can achieve significant vibration suppression of a continuous beam by adjusting the anti-frequency point and response amplitude. In this section, we study the vibration suppression effects of multiple TDVAs on the flexible beam.

The schematic diagram of the flexible beam with periodically attached TDVAs is shown in Fig. 6. As shown in Fig. 6, the coupling spring between the LRs and the beam is linear. For each local LR, the time-delayed control is applied in the coupling section.

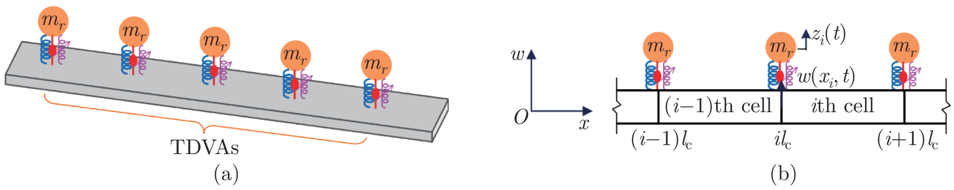

Fig. 6 (a) Schematic diagram of the flexible beam with periodically attached TDVAs. (b) Computational model of the flexible beam with TDVAs as the LRs (color online)

For a continuous beam, the TDVAs serve as the LRs, and then, a quasi-periodic structure is constructed by the continuous beam with the multiple TDVAs. For the challenge of broadband vibration suppression in low-frequency band, the optimal method for the TDFC is provided.

3.1 Bandgaps of the infinite model

For the continuous beam, the deflection of the beam can be assumed as $w(x,t) = W(x)\mathrm{e}^{\mathrm{j}\omega t}$, where $W(x)$ is the assumed mode shape function, and $\mathrm{e}^{\mathrm{j}\omega t}$ represents the dynamic response. The assumed mode shape function $W(x)$ is written as

$$W(x) = \alpha_1 \cos(\beta x) + \alpha_2 \sin(\beta x) + \alpha_3 \cosh(\beta x) + \alpha_4 \sinh(\beta x). \tag{10}$$

In Eq. (10), the coefficients α_1, α_2, α_3, and α_4 are unknown, and $\beta^4 = \frac{\rho A}{EI}\omega^2$. The mode shape function for the ith unit is

$$W_i(x') = \alpha_{1i} \cos(\beta x') + \alpha_{2i} \sin(\beta x') + \alpha_{3i} \cosh(\beta x') + \alpha_{4i} \sinh(\beta x'), \tag{11}$$

where $x' = x - il_\mathrm{c}$, $il_\mathrm{c} \leqslant x \leqslant (i+1)l_\mathrm{c}$, and l_c is the length of each unit.

For the ith delayed LR, the governing equation is given as

$$m_r\ddot{z}_i(t)+k_r(z_i(t)-w(x_i,t))+gk_r(z_i(t-\tau)-w(x_i,t-\tau))=0, \tag{12}$$

where $k_r(z_i(t)-w(x_i,t))$ is the coupling force of the connecting spring, and $gk_r(z_i(t-\tau)-w(x_i,t-\tau))$ is the active control force provided by the ith delayed LR. The symbol g denotes the control gain, and τ is the time delay. The response of the ith delayed LR is assumed as $z_i(t)=Z_i\mathrm{e}^{\mathrm{j}\omega t}$. Substituting the assumption solution $z_i(t)$ into Eq. (12) yields

$$-\omega^2m_rZ_i+k_r(Z_i-W_i(0))+gk_r(Z_i-W_i(0))\mathrm{e}^{-\mathrm{j}\omega\tau}=0, \tag{13}$$

$$Z_i=\frac{k_r+gk_r\mathrm{e}^{-\mathrm{j}\omega\tau}}{k_r-\omega^2m_r+g\mathrm{e}^{-\mathrm{j}\omega\tau}}W_i(0). \tag{14}$$

The coupling force between the delayed LR and the beam is defined as

$$\begin{aligned}f(x_i,z_i,t;\tau)&=k_r(Z_i-W_i(0))\mathrm{e}^{\mathrm{j}\omega t}+gk_r(Z_i-W_i(0))W_i(0)\mathrm{e}^{\mathrm{j}\omega(t-\tau)}\\&=(k_r+gk_r\mathrm{e}^{-\mathrm{j}\omega\tau})\frac{\omega^2m_r}{k_r-\omega^2m_r+gk_r\mathrm{e}^{-\mathrm{j}\omega\tau}}W_i(0)\mathrm{e}^{\mathrm{j}\omega t}\\&=F_{ir}\mathrm{e}^{\mathrm{j}\omega t},\end{aligned} \tag{15}$$

where F_{ir} is the amplitude of the coupling force.

The continuous conditions of the displacement, slope, bending moment, and shear force of the beam at each joint point of the delayed LR are expressed as

$$\begin{cases}W_{i-1}(l_\mathrm{c})=W_i(0), \quad W'_{i-1}(l_\mathrm{c})=W'_i(0),\\ EIW''_{i-1}(l_\mathrm{c})=EIW''_i(0), \quad EIW'''_{i-1}(l_\mathrm{c})+F_{ir}=EIW'''_i(0).\end{cases} \tag{16}$$

Substituting Eqs. (11) and (12) into Eq. (16) yields

$$\boldsymbol{H}\boldsymbol{\psi}_{i-1}=\boldsymbol{G}\boldsymbol{\psi}_i, \tag{17}$$

where

$$\begin{cases}\boldsymbol{\psi}_i=(\alpha_{1i},\alpha_{2i},\alpha_{3i},\alpha_{4i}),\\ \boldsymbol{H}=\begin{pmatrix}c & s & ch & sh\\ -\beta s & \beta c & \beta sh & \beta ch\\ -\beta^2c & -\beta^2s & \beta^2ch & \beta^2sh\\ \beta^3s & -\beta^3c & \beta^3sh & \beta^3ch\end{pmatrix},\\ \boldsymbol{G}=\begin{pmatrix}1 & 0 & 1 & 0\\ 0 & \beta & 0 & \beta\\ -\beta^2 & 0 & \beta^2 & 0\\ -F & -\beta^3 & -F & \beta^3\end{pmatrix},\end{cases}$$

in which

$$\begin{cases}c=\cos(\beta l_\mathrm{c}), \quad s=\sin(\beta l_\mathrm{c}), \quad ch=\cosh(\beta l_\mathrm{c}), \quad sh=\sinh(\beta l_\mathrm{c}),\\ F=\dfrac{k_r+gk_r\mathrm{e}^{-\mathrm{j}\omega\tau}}{EI}\dfrac{\omega^2m_r}{k_r-\omega^2m_r+gk_r\mathrm{e}^{-\mathrm{j}\omega\tau}}.\end{cases}$$

According to the Floquet-Bloch theorem[42], the relationship between the adjacent mode shape function should satisfy the following condition:

$$\boldsymbol{\psi}_i = \mathrm{e}^{\mathrm{j}ql_\mathrm{c}}\boldsymbol{\psi}_{i-1}, \tag{18}$$

where q is the wave vector. Substituting Eq. (18) into Eq. (17) yields

$$(\boldsymbol{H} - \mathrm{e}^{\mathrm{j}ql_\mathrm{c}}\boldsymbol{G})\boldsymbol{\psi}_{i-1} = \boldsymbol{0}. \tag{19}$$

As a result, the dispersion relation of the beam can de expressed as

$$\left|\boldsymbol{H} - \mathrm{e}^{\mathrm{j}ql_\mathrm{c}}\boldsymbol{G}\right| = 0. \tag{20}$$

According to the dispersion relation in Eq. (20), the bandgap of the beam for different parameters can be obtained. First, we discuss the case for the control without time delay, i.e., the time delay τ equals zero. The bandgaps of the beam for different control gains without time delay are shown in Fig. 7.

In Fig. 7, the solid lines denote the real wave vectors, and the shadows are the bandgaps. In the bandgaps, the wave propagation is completely eliminated. When the control gain g decreases from 0.9 to −0.9, although the bandgap shifts to the low-frequency range, its width

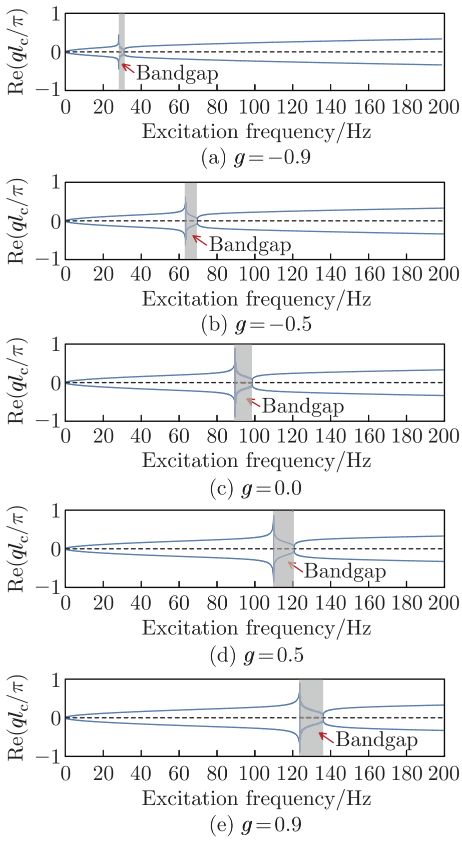

Fig. 7 Bandgaps (represented by shadows) of the beam under different control gains g, where solid lines represent the real wave vectors (color online)

gets narrower. Based on Ref. [43], the ending frequency of the bandgap can be theoretically obtained as

$$\omega_{\mathrm{e}} = \omega_r \sqrt{1 + m_r/(\rho A l_{\mathrm{c}})}, \tag{21}$$

where

$$\omega_r = \sqrt{k_r(1+g)/m_r}.$$

Actually, the stiffness of the coupling spring between the beam and the LR has the similar influence to the control gain g on the ending frequency of the bandgap. For smaller g or k_r, the bandgap moves to the lower frequency range. The relation between the control gain g and the beginning and ending frequencies of the bandgaps is shown in Fig. 8.

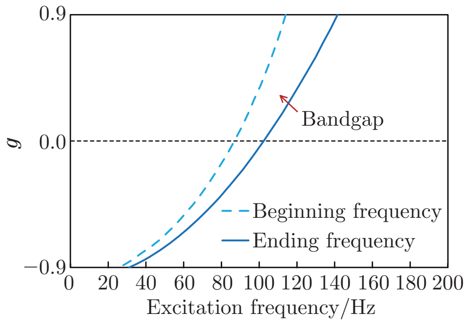

Fig. 8 Beginning and ending frequencies of the bandgap for different control gains g, where dashed lines represent the beginning frequencies obtained by numerical simulation, and solid lines represent the ending frequencies ω_{e} as defined in Eq. (21) (color online)

As shown in Fig. 8, with the decrease in the control gain g, the bandgap could shift to lower frequency region. However, as shown in Fig. 7, the bandwidth of the bandgap becomes narrower with smaller g. It indicates that the active feedback control strategy can adjust the location of the bandgap to the required frequency range. To cover the shortage that the bandwidth gets narrower for low-frequency range, the time delay should be considered.

3.2 Dynamic simplification of the beam with finite length with delayed LRs

To show the effects of time delay on both bandgap location and amplitude magnitude, the vibration response of the beam with a finite length is analyzed. F_{RF} is studied to illustrate the variation of the vibration amplitude in the concerned frequency bands. For multiple TDVAs, the governing equation of the beam is formulated as

$$EI\frac{\partial^4 w}{\partial x^4} + \rho A\frac{\partial^2 w}{\partial t^2} = f_{\mathrm{E}}(t)\delta(x-0) + \sum_{i=1}^{N} f(x_i,t)\delta(x-x_i), \tag{22}$$

where $f_{\mathrm{E}}(t)$ is the excitation force applied at the left end of the beam, N is the number of the time-delayed LRs. Similar to Eq. (12), the internal coupling force between the delayed LR and the beam is

$$f(x_i,t) = k_r(z_i(t) - w(x_i,t)) + gk_r(z_i(t-\tau) - w(x_i,t-\tau)). \tag{23}$$

The coupling force as Eq. (23) can embody the effectiveness of the coupling gain g and the time delay τ, respectively. When $\tau = 0\,\mathrm{ms}$, the magnitude of the coupling force depends on the strength of the coupling gain g. When τ is nonzero, the coupling force depends both on the coupling gain and the time delay, and the effectiveness of time delay can be clearly illustrated since the dynamic behavior of g has been known.

Based on the Galerkin truncation method, the transverse displacement of the beam is assumed as

$$w(x,t)=\sum_{p=1}^{P}\phi_p(x)q_p(t), \tag{24}$$

where P is the total number of the Galerkin truncations, $\phi_p(x)$ is the pth modal function, and $q_p(t)$ is the pth generalized displacement. Substituting Eq. (24) into Eqs. (22) and (23) yields

$$EI\sum_{p=1}^{P}\phi_p^{(4)}(x)q_p(t)+\rho A\sum_{p=1}^{P}\phi_p(x)\ddot{q}_p(t)=f_{\mathrm{E}}(t)\delta(x-0)+\sum_{i=1}^{N}f(x_i,t)\delta(x-x_i), \tag{25}$$

and the internal coupling force is written as

$$f(x_i,t)=k_r\Big(z_i(t)-\sum_{p=1}^{P}\phi_p(x_i)q_p(t)\Big)+gk_r\Big(z_i(t-\tau)-\sum_{p=1}^{P}\phi_p(x_i)q_p(t-\tau)\Big). \tag{26}$$

Multiplying Eq. (25) by the nth modal function and integrating it from 0 to the length of the beam L yield

$$\begin{aligned}&EI\sum_{p=1}^{P}\int_0^L\phi_p^{(4)}(x)\phi_n(x)\mathrm{d}xq_p(t)+\rho A\sum_{p=1}^{P}\int_0^L\phi_p(x)\phi_n(x)\mathrm{d}x\ddot{q}_p(t)\\&=\int_0^L\phi_n(x)\delta(x-0)\mathrm{d}xf_{\mathrm{E}}(t)+\sum_{i=1}^{N}\int_0^L\phi_n(x)\delta(x-x_i)f(x_i,t)\mathrm{d}x.\end{aligned} \tag{27}$$

The modal functions are selected as those for the Euler beams with the free-free end boundary. Due to the orthogonality of the modal functions and considering the modal damping of the beam and the resonators, Eq. (27) can be formulated as

$$m_p\ddot{q}_p+c_p\dot{q}_p+k_pq_p=\phi_p(0)f_{\mathrm{E}}(t)+\sum_{i=1}^{N}\phi_p(x_i)f_{\mathrm{d}}(x_i,t)+\sum_{i=1}^{N}\phi_p(x_i)f(x_i,t), \tag{28}$$

where

$$m_p=\rho A\int_0^L\phi_p^2(x)\mathrm{d}x,\quad k_p=EI\int_0^L\phi_p^{(4)}\phi_p(x)\mathrm{d}x,\quad c_p=2\zeta_p\sqrt{m_pk_p},$$

in which ζ_p is the damping ratio of the pth beam mode.

The governing equation of the ith delayed LR is expressed as

$$m_r\ddot{z}_i(t)+f_{\mathrm{d}}(x_i,t)+f(x_i,t)=0. \tag{29}$$

In Eqs. (28) and (29), the equivalent damping force f_{d} is given as

$$f_{\mathrm{d}}(x_i,t)=2\zeta_r\sqrt{m_rk_r}\Big(\dot{z}_i(t)-\sum_{p=1}^{P}\phi_p(x_i)\dot{q}_p(t)\Big), \tag{30}$$

where ζ_r is the damping ratio of each delayed LR. The displacement of the ith delayed LR is assumed as

$$z_i(t)=c_i\sin(\omega t)+d_i\cos(\omega t). \tag{31}$$

Substituting Eqs. (6) and (31) into Eqs. (28) and (29) yields $(P+N)$ equations. Then, collect the coefficients of $\sin(\omega t)$ and $\cos(\omega t)$, and be sure that their coefficients are zero. Then, $2(P+N)$ equations related to the amplitudes a_p, b_p, c_i, d_i and the excitation amplitude f_{E} are obtained. Rearranging them, one gets

$$\boldsymbol{C}_{2(P+N)\times 2(P+N)}\boldsymbol{A}_{2(P+N)\times 1} = \boldsymbol{E}_{2(P+N)\times 1}, \tag{32}$$

where $\boldsymbol{A}_{2(P+N)\times 1}$ $(= (a_1, b_1, \cdots, a_P, b_P, c_1, d_1, \cdots, c_N, d_N)^{\mathrm{T}})$ is the vector of the generalized displacement amplitudes of cosines and sines, and $\boldsymbol{C}_{2(P+N)\times 2(P+N)}$ and $\boldsymbol{E}_{2(P+N)\times 1}$ are similar to those in Eq. (7).

3.3 Vibration suppression effects for multiple TDVAs

3.3.1 F_{RF} without time delay

In this case, the number of the Galerkin truncations is set as $P = 8$, and the number of TDVAs is also selected as $N = 8$. Figure 9 shows the F_{RF} results for different control gains g without time delay. To understand the evolutionary process of the bandgaps with the control gain g, a three-dimensional (3D) view of F_{RF} and the density visualization are displayed in Fig. 9. For the control without time delay, based on Eq. (32), the F_{RF} results of the beam can be calculated to verify the bandgap structures in Subsection 3.1.

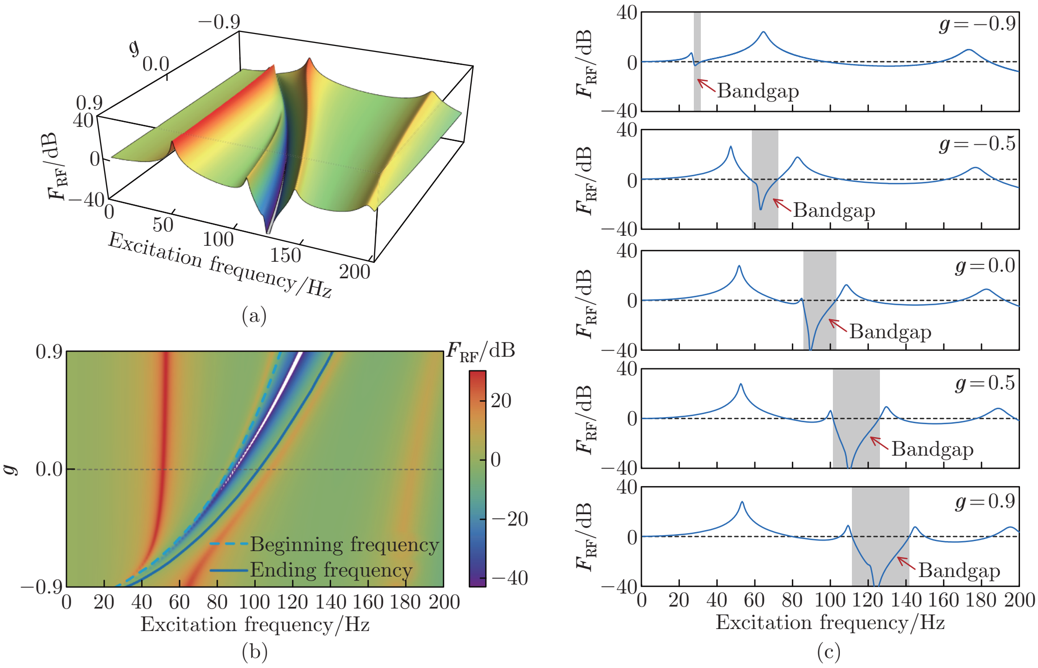

Fig. 9 (a) 3D version of the beam F_{RF} for different control gains calculated by the Galerkin truncation method. (b) Density visualization of F_{RF}. (c) F_{RF} (solid lines) and bandgap results (shadows) for $g = -0.9$, $g = -0.5$, $g = 0$, $g = 0.5$, and $g = 0.9$ (color online)

In Fig. 9(a), the F_{RF} results in the colored region below zero are in the bandgap frequency range, and the regions with warm color denote the resonance peaks. As shown in Fig. 9(a), there exists a valley between the second and third peaks in the F_{RF} results, indicating the bandgap of the beam. Figure 9(b) reveals excellent agreement with the F_{RF} results shown in Fig. 9(a). In Fig. 9(b), with the decrease in the control gain, both the beginning and ending frequencies decrease. In the density visualization of F_{RF}, the white region represents the extremely low response amplitude in the bandgap. Figures 9(a) and 9(b) show that, with the decrease in the control gain g, the frequencies of the peaks and valley shift to the lower frequency ranges gradually. Although the results demonstrate that the proper value of the control gain g can tune the location of the bandgap in the required range, the bandgap for effective vibration suppression becomes narrower.

Figure 9(c) shows the variations of the bandgap and response amplitude. In conformity with the results shown in Figs. 9(a) and 9(b), the F_{RF} results in Fig. 9(c) show that the bandgaps shift to the low-frequency range and the bandwidth is reduced when the control gain decreases.

From the results in Figs. 7 and 9(c), we can see that there exists a little difference in the bandgaps due to the existence of damping. The bandgaps in Fig. 9(c) are wider than the bandgaps in Fig. 7, since the damping further suppresses the response amplitudes and broaden the boundaries of the bandgaps. This enlightens us that the damping may play an important role in the enlargement of the gap bandwidth. Notably, there remain wide plain valleys between the first and second peaks or the third and fourth peaks. Thus, if the peaks could be eliminated and the valleys could be joined together, the useful bandwidth for vibration attenuation would be sufficiently expanded. It is worth a trial to introduce damping by adopting the time delay mechanism. The time delay mechanism has been analyzed in the literature, and it has been summarized that TDFC provides tunable coupling stiffness. The position and width of the bandgap are potentially tunable at the mean time for proper control gain and time delay.

3.3.2 F_{RF} with time delay

As mentioned above, the TDFC may lead to the convergence of the bandgaps and regions below zero between peaks. The effects of time delay on F_{RF} are analyzed. The F_{RF} results of the TDVA-coupled beam for different time delays are shown in Fig. 10 to show the effects of time delay on the elimination of peaks and joining of useful frequency bands.

Figure 10 shows the F_{RF} results at the end of the beam with different time delays when

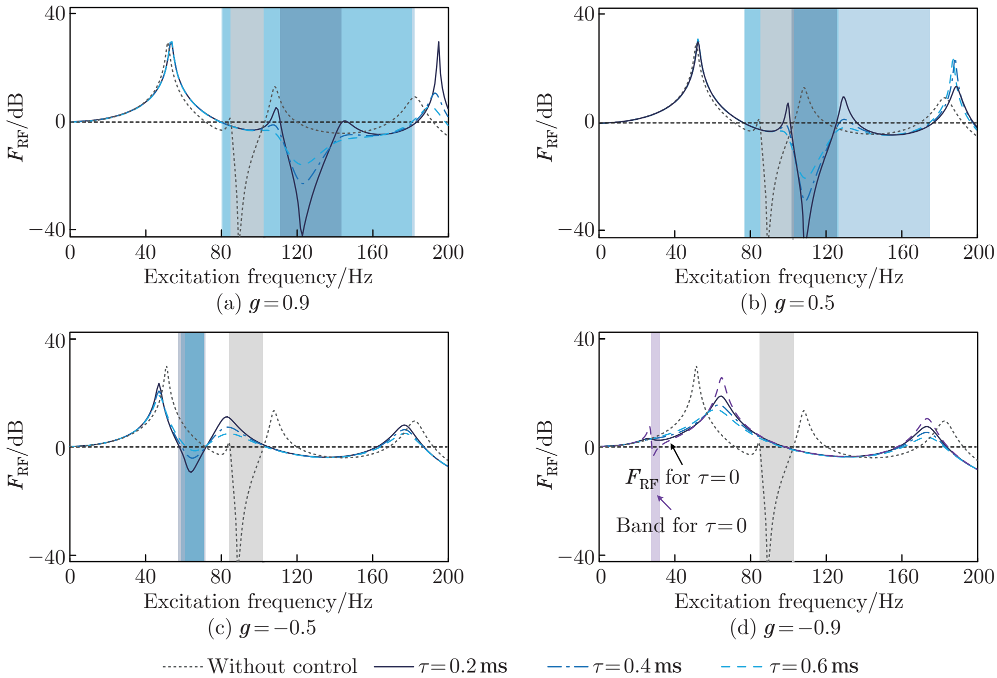

Fig. 10 F_{RF} results of the TDVA-coupled beam for different time delays calculated by the Galerkin truncation method under different control gains g, where dashed lines denote the case without control and shadows denote the continuous frequency band below zero (color online)

$g \in [-0.9, 0.9]$. The dashed line denotes the F_{RF} results without control, and the solid lines with thick, medium, and light colors indicate the cases for different time delays. The shadows with the corresponding colors show the continuous frequency bands in which F_{RF} is below zero. As shown in Fig. 10, for cases without control, the bandgap is in the range of $[85.3, 103.2]$ Hz. In Fig. 10(a), with the gradual increase in the time delay, the peaks of the response on both sides of the effective bandwidth decrease gradually, and finally fall below zero when the time delay τ increases to 0.6 ms. The band for effective vibration suppression is increased from $[100, 142]$ Hz to $[80, 182]$ Hz, which completely covers the bandgap without control. The reason is that the time delay increases the damping of the system and reduces the amplitude of the formant. Thus, the effective vibration suppression bands outside the band gap merges with it and forms a wider continuous effective band. However, the damping caused by time delay weakens the effects of vibration suppression in the band gap. Similarly, in Figs. 10(b) and 10(c), the introduction of time delay also broadens the effective frequency band, and weakens the suppression effect of vibration in the band gap. It is discovered that the bandgap can be adjusted into a low-frequency band unloosing its width. In Fig. 10(d), due to the large control gain, it is difficult to find an appropriate time delay to improve the damping effect of the TDVA on beam vibration. Objectively, it is found that the improvement of the vibration suppression effect of the beam by introducing time delay control is not universal. From the above analysis, we find that TDFC is effective in the ascension of the vibration absorption inhibition effect and the change of the effective vibration suppression band position, and broadening the effective vibration suppression has effects on problems such as bandwidth.

Figure 11 shows the trends of the F_{RF} value at the end of the beam with the control gain under different time delays τ. The dotted lines show the boundaries where $F_{\mathrm{RF}} = 0$, the warm tone is the part where $F_{\mathrm{RF}} > 0$, and the cool tone is the part where $F_{\mathrm{RF}} < 0$. It can be seen that when the time delay is small, the peaks on the right side of the band gap can gradually disappear. For example, when $g = 0.9$, the response of the beam has a peak near 145 Hz in the absence of time delay (see Fig. 9). However, in Fig. 11, within the range of $[0.4, 3.6]$ ms, the peak near 145 Hz is weakened, which can generate a very wide continuous effective vibration suppression frequency band. By comparing Figs. 11(a), 11(b), 11(c), and 11(d), it is found that the effect of g on the position of the effective vibration suppression band is qualitatively different under different time delays. Therefore, the control gain and time delay should be considered simultaneously to improve the vibration suppression effects of the vibration absorber on the beam.

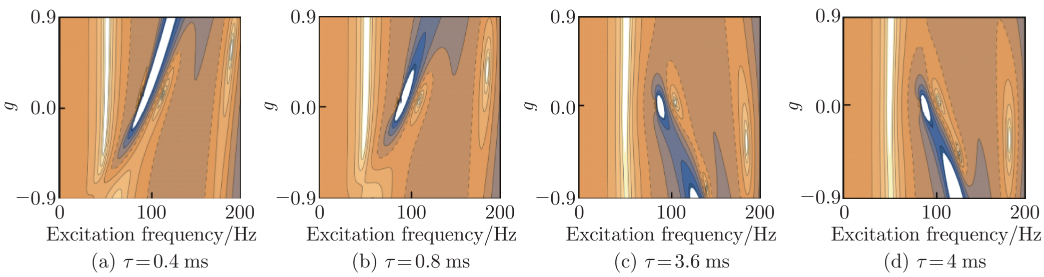

Fig. 11 F_{RF} results at the end of the beam with respect to the control gain g under different time delays τ (color online)

Figure 12 shows the trends of F_{RF} at the end of the beam with the time delay τ under different control gains g. Similarly, the dotted line is the dividing line where $F_{\mathrm{RF}} = 0$, the warm tone is the part where $F_{\mathrm{RF}} > 0$, and the cool tone is the part where $F_{\mathrm{RF}} < 0$. From Fig. 12, it can be seen that the time delay has different effects on the amplitude-frequency evolution under different control gains. When $g = -0.3$, the peak near 95 Hz gradually disappears with

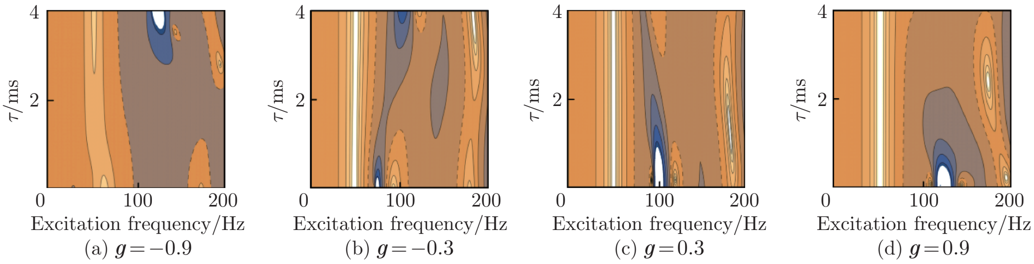

Fig. 12 F_{RF} results at the end of the beam with respect to the time delay τ under different control gains g (color online)

the increase in the time delay, and the effective bandwidths on both sides merge and form a continuous effective vibration suppression band, in which $F_{\mathrm{RF}} \geqslant 0$. Similarly, when $g = 0.3$, the peak near 130 Hz gradually disappears with the increase in the time delay, forming a continuous effective vibration suppression band. It can be seen that the time delay can greatly widen the effective vibration suppression band by weakening the F_{RF} value at the formant.

3.4 Effects of the number of multiple TDVAs

In the above sections, the number of TDVAs is set as $P = 8$ in the exploration of the effects of TDFC on the bandgaps and responses of the beam. According to the results in Section 3, the number of LRs without control has little influence on the position of the bandgaps. However, in our research process, it is found that the number of TDVAs has a great effect on the width of the effective frequency band and the response amplitude of the beam in the effective frequency band.

Figure 13 shows the effects of the number of TDVAs on the bandwidth of the beam bandgap for vibration suppression. In Fig. 13, the number of TDVAs is chosen as $N = 4$, $N = 8$, and $N = 16$. It can be clearly seen from Fig. 13 that the number of TDVAs plays an important role in broadening the effective bandwidth and improving the vibration suppression effect within the effective frequency band. For a larger number of TDVAs, a better vibration suppression effect and a wider effective bandwidth are achieved. The increase in N can broaden the effective vibration suppression band and reduce the amplitude in the band. When the number of TDVAs applied on the continuous beam increases, the sum mass of absorbers becomes larger, and correspondingly, more effective mass is involved into the vibration suppression. In addition, when the number of TDVAs is the same, the vibration suppression band can be effectively widened by introducing TDFC, which confirms the results in Fig. 10. This is because of the larger control interaction force and the equivalent LR mass brought by the time-delayed control for vibration suppression. Based on the results in Figs. 10 and 13, we can see that time delay can break the contradiction between low-frequency and broadband vibration suppression. In practical engineering, it is necessary to select the appropriate number of TDVAs according to the engineering demand and cost.

4 Conclusions and discussion

In this study, the effects of TDVA on the vibration suppression of a continuous beam are studied. First, the vibration suppression effect of a single TDVA on the beam is studied. The results show that the introduction of TDFC is beneficial to improving the vibration suppression on the beam in the anti-resonance region. Then, considering multiple TDVAs uniformly distributed on the beam, the relationship between the response features of the beam and the TDFC parameters is given. The main contributions of this study are summarized as follows.

(i) For a continuous beam, TDVA is introduced to improve the vibration suppression effects.

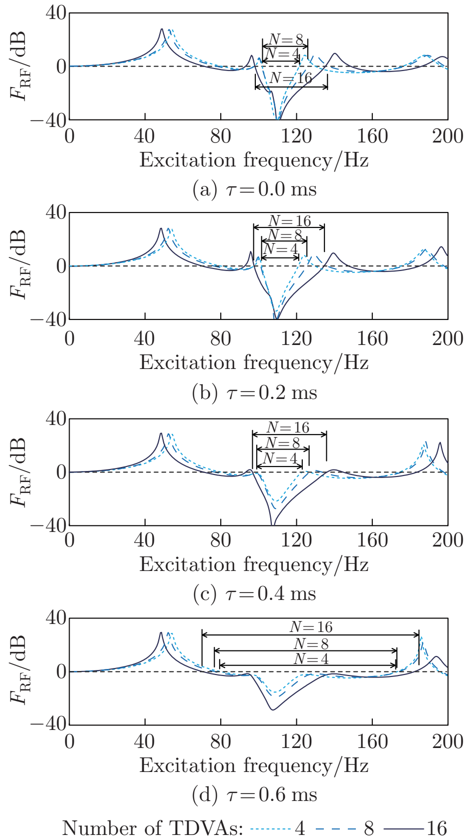

Fig. 13 Effects of the number of TDVAs on the effective frequency band of beam vibration suppression under different time delays τ when $g = 0.5$ (color online)

When a single TDVA is applied, the anti-resonance at a specific external excitation frequency can be realized through the optimization design of TDFC parameters. The analysis of the dynamic behaviors based on the general dynamic model of the coupling system discovers that time delay can adjust the location of the anti-frequency point and reduce the response amplitude at the anti-frequency point simultaneously, which can achieve the optimum vibration suppression at a required frequency point.

(ii) The vibration suppression effect of multiple TDVAs is studied when they are uniformly distributed on the continuous beam. Utilizing the Floquet-Bloch theorem, the location and bandwidth of the bandgap can be theoretically described by different structural parameters, and the relationship between the bandgap and the control parameters is obtained. The influence rules of the TDFC on the vibration suppression effectiveness of the continuous beam are given. When multiple TDVAs are applied, appropriate TDC parameters are obtained to adjust the position of the effective vibration suppression band and widen its bandwidth.

(iii) Based on the analysis of the effects of single and multiple TDVAs on the vibration suppression effectiveness of a continuous beam, the corresponding optimization or design criteria are proposed for appropriate TDFC parameters. In addition, the variations of the location and bandwidth of bandgap with the number of TDVAs are given. It is revealed that the TDVAs have a significant vibration suppression effect since when the number of TDVAs increases, the bandgap is considerably widened, and the contradiction between the low-frequency and broad bandgaps is overcome.

The research results in this study show that the TDVA has a good effect on the vibration suppression of continuous beams. Time delay can simultaneously adjust the location and bandwidth of the bandgap, and thus, it can break through the contradiction of the low-frequency and extension of the bandgap. In this study, the method of parameter selection for the application of TDVAs in the beam structure is presented theoretically, which provides guidance for the applications of TDVAs in bridge, aerospace, and other practical projects. In the future work, the effects of nonlinear coupling and sum mass of TDVAs for nonlinear continuous beams will be considered for wide and low-frequency vibration suppression.

Conflict of interest The authors declare no conflict of interest.

Data availability All data generated or analysed during this study are included in this published article.

References

[1] DEN HARTOG, J. P. *Mechanical Vibrations*, Dover Publications, Inc., New York (1985)

[2] XIAO, J., ZHANG, Q., LIU, H., HUANG, T., and SHAN, X. Research on vibration suppression by a multi-point flexible following support head in thin-walled parts mirror milling. *The International Journal of Advanced Manufacturing Technology*, **106**, 3335–3344 (2020)

[3] MORADI, H., VOSSOUGHI, G., BEHZAD, M., and MOVAHHEDY, M. R. Vibration absorber design to suppress regenerative chatter in nonlinear milling process: application for machining of cantilever plates. *Applied Mathematical Modelling*, **39**(2), 600–620 (2015)

[4] ZHANG, J. H., GUO, P., LIN, J. W., and WANG, K. N. A mathematical model for coupled vibration system of road vehicle and coupling effect analysis. *Applied Mathematical Modelling*, **40**(2), 1199–1217 (2016)

[5] ZHAO, P. C., ZHANG, K., ZHAO, C., and DENG, Z. C. Multi-resonator coupled metamaterials for broadband vibration suppression. *Applied Mathematics and Mechanics* (*English Edition*), **42**(1), 53–64 (2021) https://doi.org/10.1007/s10483-021-2684-8

[6] XIE, F. and ALY, A. M. Structural control and vibration issues in wind turbines: a review. *Engineering Structures*, **210**, 110087 (2020)

[7] YANG, F., SEDAGHATI, R., and ESMAILZADEH, E. Vibration suppression of structures using tuned mass damper technology: a state-of-the-art review. *Journal of Vibration and Control*, **28**(7-8), 812–836 (2022)

[8] BATOU, A. and ADHIKARI, S. Optimal parameters of viscoelastic tuned-mass dampers. *Journal of Sound and Vibration*, **445**, 17–28 (2019)

[9] CASALOTTI, A., EI-BORGI, S., and LACARBONARA, W. Metamaterial beam with embedded nonlinear vibration absorbers. *International Journal of Non-Linear Mechanics*, **98**, 32–42 (2018)

[10] GENG, X. F., DING, H., WEI, K. X., and CHEN, L. Q. Suppression of multiple modal resonances of a cantilever beam by an impact damper. *Applied Mathematics and Mechanics* (*English Edition*), **41**(3), 383–400 (2020) https://doi.org/10.1007/s10483-020-2588-9

[11] WEBER, F. Semi-active vibration absorber based on real-time controlled MR damper. *Mechanical Systems and Signal Processing*, **46**(2), 272–288 (2014)

[12] ZHANG, B. L., HAN, Q. L., and ZHANG, X. M. Recent advances in vibration control of offshore platforms. *Nonlinear Dynamics*, **89**(2), 755–771 (2017)

[13] CHEN, J. N., ZHANG, W., LIU, J., and HU, W. H. Vibration absorption of parallel-coupled nonlinear energy sink under shock and harmonic excitations. *Applied Mathematics and Mechanics* (*English Edition*), **42**(8), 1135–1154 (2021) https://doi.org/10.1007/s10483-021-2757-6

[14] BROWNE, F., REES, B., CHIU, G. T. C., and JAIN, N. Iterative learning control withtime-delay compensation: an application to twin-roll strip casting. *IEEE Transactions on Control Systems Technology*, **29**(1), 140–149 (2021)

[15] MAZENC, F., MALISOFF, M., and BHOGARAJU, I. N. S. Sequential predictors for delay compensation for discrete time systems with time-varying delays. *Automatica*, **122**, 109188 (2020)

[16] PYRAGAS, K. Control of chaos via an unstable delayed feedback controller. *Physical Review Letters*, **86**(11), 2265–2268 (2001)

[17] LIAO, X. X. and CHEN, G. R. Chaos synchronization of general Lur'e systems via time-delay feedback control. *International Journal of Bifurcation and Chaos*, **13**(1), 207–213 (2003)

[18] WANG, Q. and WANG, Z. H. Optimal feedback gains of a delayed proportional-derivative (PD) control for balancing an inverted pendulum. *Acta Mechanica Sinica*, **33**(3), 635–645 (2017)

[19] XU, Q., STEPAN, G., and WANG, Z. H. Balancing a wheeled inverted pendulum with a single accelerometer in the presence of time delay. *Journal of Vibration and Control*, **23**(4), 604–614 (2017)

[20] LIU, K., CHEN, L. X., and CAI, G. P. Experimental study of active control for a flexible beam with nonlinear hysteresis and time delay. *Journal of Vibration and Control*, **22**(3), 722–735 (2016)

[21] ZHANG, T., LI, H. G., and CAI, G. P. Time delay stability analysis for vibration suppression of a smart cantilever beam with hysteresis property. *Journal of Low Frequency Noise Vibration and Active Control*, **40**(2), 898–915 (2021)

[22] RUSINEK, R., MITURA, A., and WARMINSKI, J. Time delay Duffing's systems: chaos and chatter control. *Meccanica*, **49**(8), 1869–1877 (2014)

[23] LEHOTZKY, D., INSPERGER, T., and STEPAN, G. Numerical methods for the stability of time-periodic hybrid time-delay systems with applications. *Applied Mathematical Modelling*, **57**, 142–162 (2018)

[24] SUN, X. T. and XU, J. Vibration control of nonlinear absorber-isolator-combined structure with time-delayed coupling. *International Journal of Non-Linear Mechanics*, **83**, 48–58 (2016)

[25] SUN, X. T., ZHANG, S., and XU, J. Parameter design of a multi-delayed isolator with asymmetrical nonlinearity. *International Journal of Mechanical Sciences*, **138**, 398–408 (2018)

[26] SUN, X. T., WANG, F., and XU, J. Dynamics and realization of a feedback-controlled nonlinear isolator with variable time delay. *Journal of Vibration and Acoustics-Transactions of the ASME*, **141**(2), 021005 (2019)

[27] EL-SAYED, A. T. and BAUOMY, H. S. Vibration control of helicopter blade flapping via time-delay absorber. *Meccanica*, **49**(3), 587–600 (2014)

[28] SAEED, N. A. and EL-GANAINI, W. A. Utilizing time-delays to quench the nonlinear vibrations of a two-degree-of-freedom system. *Meccanica*, **52**(11-12), 2969–2990 (2017)

[29] YANG, T. and CAO, Q. J. Nonlinear transition dynamics in a time-delayed vibration isolator under combined harmonic and stochastic excitations. *Journal of Statistical Mechanics-Theory and Experiment*, **2017**, 043202 (2017)

[30] YANG, T. and CAO, Q. J. Delay-controlled primary and stochastic resonances of the SD oscillator with stiffness nonlinearities. *Mechanical Systems and Signal Processing*, **103**, 216–235 (2018)

[31] OLGAC, N. and HOLMHANSEN, B. T. A novel active vibration absorption technique-delayed resonator. *Journal of Sound and Vibration*, **176**(1), 93–104 (1994)

[32] OLGAC, N., ELMALI, H., and VIJAYAN, S. Introduction to the dual frequency fixed delayed resonator. *Journal of Sound and Vibration*, **189**(3), 355–367 (1996)

[33] JALILI, N. and OLGAC, N. Multiple delayed resonator vibration absorbers for multi-degree-of-freedom mechanical structures. *Journal of Sound and Vibration*, **223**(4), 567–585 (1999)

[34] HOSEK, M., OLGAC, N., and ELMALI, H. The centrifugal delayed resonator as a tunable torsional vibration absorber for multi-degree-of-freedom systems. *Journal of Vibration and Control*, **5**(2), 299–322 (1999)

[35] HOSEK, M., ELMALI, H., and OLGAC, N. A tunable torsional vibration absorber: the centrifugal delayed resonator. *Journal of Sound and Vibration*, **205**(2), 151–165 (1997)

[36] SUN, Y. X. and XU, J. Experiments and analysis for a controlled mechanical absorber considering delay effect. *Journal of Sound and Vibration*, **339**, 25–37 (2015)

[37] XU, J. and SUN, Y. X. Experimental studies on active control of a dynamic system via a time-delayed absorber. *Acta Mechanica Sinica*, **31**(2), 229–247 (2015)

[38] WANG, F. and XU, J. Parameter design for a vibration absorber with time-delayed feedback control. *Acta Mechanica Sinica*, **35**(3), 624–640 (2019)

[39] WANG, F., SUN, X. T., MENG, H., and XU, J. Time-delayed feedback control design and its application for vibration absorption. *IEEE Transactions on Industrial Electronics*, **68**(9), 8593–8602 (2021)

[40] WANG, F., SUN, X. T., MENG, H., and XU, J. Tunable broadband low-frequency band gap of multiple-layer metastructure induced by time-delayed vibration absorbers. *Nonlinear Dynamics*, **107**(3), 1903–1918 (2022)

[41] ZHANG, X. X., XU, J., and JI, J. C. Modelling and tuning for a time-delayed vibration absorber with friction. *Journal of Sound and Vibration*, **424**, 137–157 (2018)

[42] ZHANG, X. X., XU, J., and FENG, Z. C. Nonlinear equivalent model and its identification for a delayed absorber with magnetic action using distorted measurement. *Nonlinear Dynamics*, **88**(2), 937–954 (2017)

[43] MENG, H., SUN, X. T., XU, J., and WANG, F. The generalization of equal-peak method for delay-coupled nonlinear system. *Physica D-Nonlinear Phenomena*, **403**, 132340 (2020)

[44] MENG, H., SUN, X. T., XU, J., and WANG, F. Establishment of the equal-peak principle for a multiple-DOF nonlinear system with multiple time-delayed vibration absorbers. *Nonlinear Dynamics*, **104**(1), 241–266 (2021)

[45] JI, J. C. and ZHANG, N. Suppression of the primary resonance vibrations of a forced nonlinear system using a dynamic vibration absorber. *Journal of Sound and Vibration*, **329**(11), 2044–2056 (2010)

[46] JI, J. C. and ZHANG, N. Suppression of super-harmonic resonance response using a linear vibration absorber. *Mechanics Research Communications*, **38**(6), 411–416 (2011)

[47] QIAN, Y. J., CUI, Q. D., YANG, X. D., and ZHANG, W. Manipulating transverse waves through 1D metamaterial by longitudinal vibrations. *International Journal of Mechanical Sciences*, **168**, 105296 (2020)

[48] WANG, Q., LI, J. Q., ZHANG, Y., XUE, Y., and LI, F. M. Bandgap properties in metamaterial sandwich plate with periodically embedded plate-type resonators. *Mechanical Systems and Signal Processing*, **151**, 107375 (2021)

[49] FAN, J. X., SONG, B., ZHANG, L., WANG, X. B., ZHANG, Z., WEI, S. S., XIANG, X., ZHU, X. F., and SHI, Y. S. Structural design and additive manufacturing of multifunctional metamaterials with low-frequency sound absorption and load-bearing performances. *International Journal of Mechanical Sciences*, **238**, 107848 (2023)

[50] GAO, Y. Q. and WANG, L. F. Active multifunctional composite metamaterials with negative effective mass density and negative effective modulus. *Composite Structures*, **291**, 115586 (2022)

[51] ZHOU, J. X., WANG, K., XU, D. L., and OUYANG, H. J. Local resonator with high-static-low-dynamic stiffness for lowering band gaps of flexural wave in beams. *Journal of Applied Physics*, **121**(4), 044902 (2017)

[52] WANG, Z. W., ZHANG, Q., ZHANG, K., and HU, G. K. Tunable digital metamaterial for broadband vibration isolation at low frequency. *Advanced Materials*, **28**(44), 9857–9861 (2016)

[53] BANERJEE, A. Non-dimensional analysis of the elastic beam having periodic linear spring mass resonators. *Meccanica*, **55**(5), 1181–1191 (2020)

[54] YAN, G. W., YAO, S., LI, Y. L., and ZHOU, W. X. Topological optimization of thin elastic metamaterial plates for ultrawide flexural vibration bandgaps. *International Journal of Mechanical Sciences*, **242**, 108014 (2023)

[55] YI, K. J., OUISSE, M., SADOULET-REBOUL, E., and MATTEN, G. Active metamaterials with broadband controllable stiffness for tunable band gaps and non-reciprocal wave propagation. *Smart Materials and Structures*, **28**(6), 065025 (2019)

[56] HE, Z. H., WANG, Y. Z., and WANG, Y. S. Active feedback control of effective mass density and sound transmission on elastic wave metamaterials. *International Journal of Mechanical Sciences*, **195**, 106221 (2021)

[57] SIROTA, L., SABSOVICH, D., LAHINI, Y., ILAN, R., and SHOKEF, Y. Real-time steering of curved sound beams in a feedback-based topological acoustic metamaterial. *Mechanical Systems and Signal Processing*, **153**, 107479 (2021)

[58] CHEN, L. X. and CAI, G. P. Design method of multiple time-delay controller for active structural vibration control. *Applied Mathematics and Mechanics* (*English Edition*), **30**(11), 1405–1414 (2009) https://doi.org/10.1007/s10483-009-1106-z

[59] GAO, Y. Q. and WANG, L. F. Broad bandgap active metamaterials with optimal time-delayed control. *International Journal of Mechanical Sciences*, **254**, 108449 (2023)